International Journal of Automotive Technology, Vol. 8, No. 3, pp. 289–298 (2007)

1229-9138/2007/034-05

SIMULATION OF STARTING PROCESS OF DIESEL ENGINE UNDER COLD CONDITIONS

J. K. PARK*

Department of Mechanical Engineering, Konkuk University, Seoul 143-701, Korea

(Received 31 July 2006; Revised 8 May 2007)

ABSTRACT–A nonlinear dynamic simulation model from cranking to idle speed is developed to optimize the cold start process of a diesel engine. Physically-based first order nonlinear differential equations and some algebraic equations describing engine dynamics and starter motor dynamics are used to model the performance of cold starting process which is very complex and involves many components including the cold start aiding method. These equations are solved using numerical schemes to describe the starting process of a diesel engine and to study the effects of cold starting parameters. The validity of this model is examined by a cold start test at –20°C. Using the developed model the effects of the important starting variables on the cold starting processes were investigated. This model can be served as a tool for designing computer aided control systems that improve cold start performance.

KEY WORDS : Dynamic modelling, Diesel starting system, Cold start, Friction torque, Starter motor

1. INTRODUCTION

Diesel engine cold start is very important in military vehicles and, generally, –32°C cold start is required. Cold start at this temperature is extremely difficult for a diesel engine and a manifold flame heater is used as cold start aid. Typically, the engine cold start process with manifold flame heater can be divided into four phases: cranking with flame heater on but no fuel injection to the cylinder; cranking with fuel injection to the cylinder; from the first firing to engine running; warm up, from engine running to the idle speed. Such transient engine starting process is a very complex process including engine, battery, starter motor, ignition and flame heater systems.

Henein and his coworks (Gardner and Henein, 1988, Liu *et al.*, 2001, 2003) have developed mathematical models of a diesel engine starting. Even though certain aspects of engine cold starter process have been reported in these literatures, a dynamic diesel engine cold starting model which involves starter motor, engine models including cold starting aiding method is not available.

The purpose of this study is to develop mathematical models of the diesel engine subsystems and the starting system during cold start to optimize the diesel engine cold starting process. First-order nonlinear differential equations and some regression models describing engine, starter motor, gas flow process, heat transfer, cylinder pressure, blowby, and engine friction will be presented. Next, a synthesis of the overall cold start model and its implementation into a computer simulation of the above mentioned four phases are illustrated. The qualitative validation of the model is carried out by comparing the numerical results with the experimental data that was obtained from an 8 cylinder, 4 stroke, direct-injection Diesel engine. Then, using the developed simulation program, the effect of blowby, intake air temperature increased by the flame heater, initial cylinder wall temperature and heat loss in the cranking process are investigated.

*Corresponding author. e-mail: jungkyup@konkuk.ac.kr

2. DESCRIPTION OF MODELS

A nonlinear dynamic model for a naturally aspirated, four-stroke, direct diesel engine is developed. It accounts for the engine dynamics of piston-connecting rod-crankshaft mechanism along with the starter dynamics and the friction losses associated with the piston assembly, engine bearing, auxiliaries and valve trains. Also, it accounts for the cylinder pressure model which deals with the gas exchange processes, blowby flow, combustion process and heat transfer.

2.1. Engine Dynamics

During cranking, the starter motor produces enough torque to overcome engine friction and drives the engine through the pinion and flywheel gears as shown in Figure 1. When the engine and starter motor are engaged, the

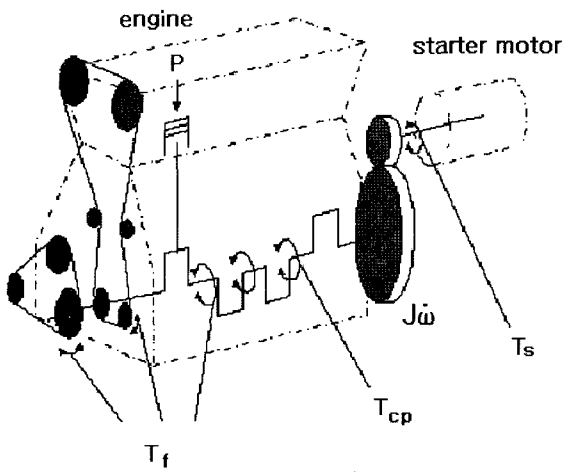

Figure 1. Schematics of engine dynamics.

system dynamics can be described by a torque balance on the engine crankshaft. By Newton's law:

$$T_{net} = K_s T_s + T_{cp} - T_f \tag{1}$$

where T_s is the starter motor torque, T_{cp} is the cylinder pressure torque, T_f is the engine friction torque and K_s is the gear ratio of the flywheel and the pinion of the start motor. The net torque T_{net} is the torque left for accelerating the engine, i.e.

$$T_{net} = J\dot{\omega} \tag{2}$$

where ω denotes engine speed and J denotes the total system inertia of the engine and starter motor. The system inertia J can be expressed in terms of the engine inertia J_e and the starter motor inertia J_s. When the starter motor and the engine are engaged,

$$J = J_e + K_s^2 J_s \tag{3}$$

Once the starter motor is disengaged from the engine,

$$J = J_e \tag{4}$$

2.2. Starter Motor Torque

The general mathematical formulation for determining the instantaneous torque of the starter motor is adopted from an empirical relationship suggested by Poublon and Patterson (1985) as:

$$T_s = C_1 e^{-C_2 N} \tag{5}$$

where N(rev/min) is the instantaneous flywheel speed. The value of C_1(=384.3) and C_2(=−0.0107) were determined by plotting the natural log of the starter motor torque during cranking against the starter speed for a number of speeds.

2.3. Engine Friction Torque

Engine friction characteristics for normal engine operating conditions have been studied (Rogenberg, 1982; Uras and Patterson, 1985; Rezeka and Henein, 1984; Shin, 2004). However, a physically based friction model at low engine speeds and low temperatures during engine cold starting is not available. In this study, different models are used for firing and non-firing period because of these limitations of these models.

For the non-firing period, the friction torque regression model suggested by Tang *et al.* (1989) is used.

$$T_f = f_1\omega + f_2\omega^2 + f_3[T_{cp} + K_s T_s] + f_4[T_{cp} + K_s T_s]^2 + f_5 \tag{6}$$

where ω is the engine speed in revolutions per minute, T_{cp} is the total cylinder pressure torque, T_s is the torque provided by the starter motor, f_1, f_2, f_3, f_4 and f_5 are the regression coefficients.

For the firing period, the friction equation developed by Rezeka and Henein (1984) is used. It accounts for the friction losses stemming from (1) the piston rings hydrodynamic lubrication regimes, (2) the piston rings mixed lubrication regimes, (3) piston skirt hydrodynamic lubrication regime, (4) valve train friction, (5) auxiliaries and unloaded bearing friction, (6) loaded bearing friction. The total instantaneous torque at any crank angle is given by

$$T_f = \Sigma a_i T_f^{(i)} \tag{7}$$

where, a_i denotes the empirical coefficients for the ith friction components, and $T_f^{(i)}$ denotes the friction correlation of the ith friction components. The terms a_i are determined by minimizing the magnitude of the error between the predicted and the measured friction torques. The reader is referred to Appendix A for the expressions of the $T_f^{(i)}$ terms.

2.4. Cylinder Pressure Torque

The total cylinder pressure torque in multicylinder engine can be expressed as

$$T_{cp}(\theta) = \sum_{i=0}^{ncyl} T_{cpi}(\theta_i) \tag{8}$$

where $T_{cpi}(\theta_i)$ is cylinder pressure torque contribution of cylinder i at given crank position angle. It can be derived from a dynamic analysis of the slider-crank mechanism. To simulate cylinder pressure torque, a thermodynamic-based engine cycle simulation is used (Heywood, 1988; Medica and Giadross, 1994). The three control volumes are the intake manifold including intake port, cylinder, and exhaust manifold including exhaust port as shown in Figure 2. Heat transfers only occur in the cylinder, intake port, and exhaust port. It is assumed that the system can be characterized by temperature T, pressure P, and the equivalence ratio ϕ.

From the continuity equation, one can write

$$\frac{dm}{dt} = \dot{m}_{in}+\dot{m}_{ex}+\dot{m}_b+\dot{m}_f \tag{9}$$

where m is the mass in the cylinder. The mass flow rate, $\dot{m}_{in}$, $\dot{m}_{ex}$, $\dot{m}_b$, $\dot{m}_f$ are determined from the gas flow through intake and exhaust valve, blowby flow and fuel injection.

From the first law of thermodynamics, one can write

$$\frac{d(mu)}{dt} = -P\frac{dV}{dt}+\dot{Q}+\sum_j h_j\dot{m}_j \tag{10}$$

where u is the specific interal energy. V is the cylinder volume, $P(dV/dt)$ is the rate of work done by the piston displacement, $\dot{Q}$ is the heat transfer across the system boundary, and h_j is the energy carried out or brought in by the flowing gas and injected liquid fuel. Applying the state equation, one obtains

$$PV = mRT \tag{11}$$

The interal energy u and gas constant R can be expressed as a function of P, T, ϕ.

$$u = u(P,T,\phi)$$

$$R = R(P,T,\phi) \tag{12}$$

The time derivative of the equivalence ratio ϕ is given by

$$\frac{d\phi}{dt} = \frac{1+\phi FA_s}{m}\left(\frac{1+\phi FA_s}{FA_s}\dot{m}_f-\phi\frac{dm}{dt}\right) \tag{13}$$

where FA_s is the stoichiometric fuel-air ratio. Combining Equations (11)~(13) with Equation (10) and rearranging the terms, one obtains

$$\frac{dT}{dt} = \left(\frac{\partial u}{\partial T}+\frac{P}{T}\frac{\partial u}{\partial P}\frac{A}{B}\right)^{-1}\left\{-\frac{P}{m}\frac{dV}{dt}+\right.$$

$$\left.\frac{1}{m}\left(\dot{Q}+\sum_j h_j\dot{m}_j-u\frac{dm}{dt}\right)-\frac{\partial u}{\partial\phi}\frac{d\phi}{dt}-C\right\} \tag{14}$$

where

$$A=1+\frac{T}{R}\frac{\partial R}{\partial T},\quad B=1-\frac{P}{R}\frac{\partial R}{\partial P}$$

$$C=\frac{P}{B}\left[\frac{1}{V}\frac{dV}{dt}-\frac{1}{m}\frac{dm}{dt}-\frac{1}{R}\frac{\partial R}{\partial\phi}\frac{d\phi}{dt}\right]\frac{\partial u}{\partial P}$$

The above cylinder temperature, equivalence ratio, and mass differential equations can be solved by numerical integration. Solving these equations requires the use of gas properties, cylinder volume, fuel burning rate correlation, mass flow rate, and heat transfer calculations. With estimated values of cylinder temperature, volume, and mass, the cylinder pressure can be estimated by using the ideal gas law.

2.4.1. Gas exchange processes

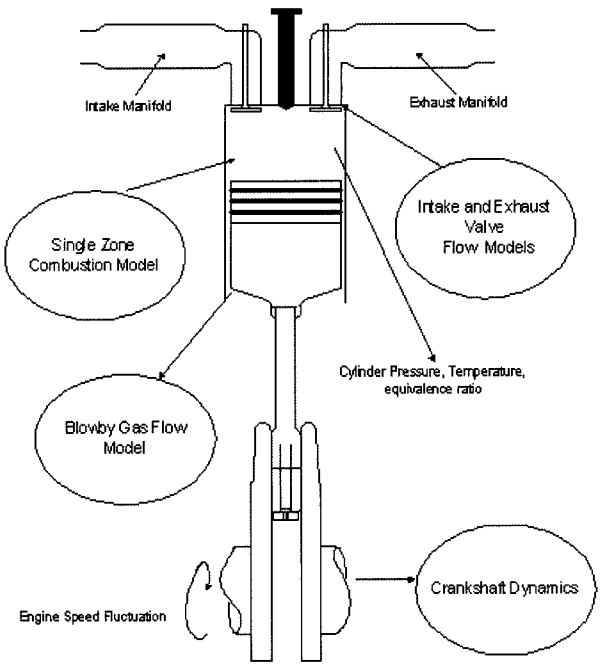

Figure 2. Schematics of three engine control volumes.

A one-dimensional quasi-steady compressible flow analysis is used to calculate the mass flow rate through the intake and exhaust valve. The manifolds are treated as infinite plenums with specified pressures, thus neglecting any dynamic effects in the flow due to pressure waves. From information on the gas conditions in the cylinder and manifolds, plus a geometric valve area and discharge coefficient, the instantaneous mass flow through the valves (and ports) can be calculated (Heywood, 1988).

2.4.2. Combustion process

The single zone model proposed by Watson *et al.* (1980) is used here because Watson's correlation is widely accepted and can be used to predict both premixed and diffusion burning rate. Several formulas have been proposed for the calculation of ignition delay in diesel engines. In this study, the ignition delay model of Hiroyasu *et al.* (1980) is used. The equilibrium combustion product gas properties were evaluated using Olikara and Borman's (1975) computer program which rapidly calculates the equilibrium mole fractions with respect to temperature, pressure and equivalence ratio for the products of combustion.

2.4.3. Heat transfer

An instantaneous convective heat transfer is defined as the form

$$\frac{dQ}{dt} = \sum_j \alpha_j A_j(T_j - T_{wall}) \tag{15}$$

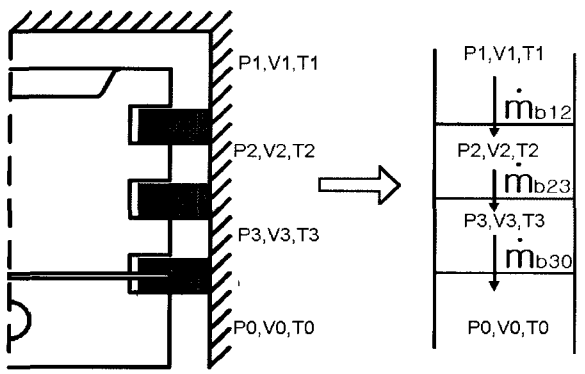

Figure 3. Model for blowby gas flow past piston rings.

T_{wall} is determined by using the heat transfer structure of the cylinder wall to the coolant or from the cylinder gas. α_j is the heat transfer coefficient and A_j is the area of each section. Woschni's correlation (1967) is used for evaluation of the cylinder heat transfer coefficient. Port heat transfer coefficients are calculated by using Caton and Heywood's (1981) correlation. Readers are referred to the Appendix B for the expression of the α_j.

2.4.4. Blowby gas flow

The blowby model (Namazian and Heywood, 1982) considers a series of interconnected volumes in the crevice region and solves the continuity equation between those regions. The ring gaps are assumed to be the only openings for the gas to leak out. The flow through ring gaps was modeled as an orifice flow. To determine the mass flow rate through the ring-side clearance, the flow is treated as an isothermal compressible flow through a narrow channel

$$\dot{m}_b = C_d A_e P_1 \sqrt{\frac{2\gamma}{\gamma-1}\left[\left(\frac{P_2}{p_1}\right)^{2/\gamma} - \left(\frac{P_2}{p_1}\right)^{(\gamma+1)/\gamma}\right]/R_1 T_1} \qquad (16)$$

where C_d is the discharge coefficient and A_e is the area of the ring gap. The mass flow, $\dot{m}_b$ is found by examining each pair of adjacent volumes in turn as shown in Figure 3. The mass and pressure changes with each volume are related by the perfect gas law:

$$dm_b = \frac{V_i}{R_1 T_{wall}} dP_i \qquad (17)$$

where V_i is the crevice volume and T_{wall} is the average wall temperature.

Equations (16) and (17) can be numerically integrated to obtain the pressure history of each volume, and more importantly, the mass flow out of the main cylinder and into the crankcase (blowby).

3. MODEL SYNTHESIS AND NUMERICAL METHOD

In the previous section, individual engine and starting subsystem models are presented. Each of these models can be described by one or more nonlinear first-order differential equations or algebraic equations. Three control volumes are considered for the individual cylinder. These 3 unknown variables (T, m, Φ) of 8 cylinder, intake manifold and exhaust manifold make 30 equations. Heat transfer rate, work rate, piston ring pressure variation rate

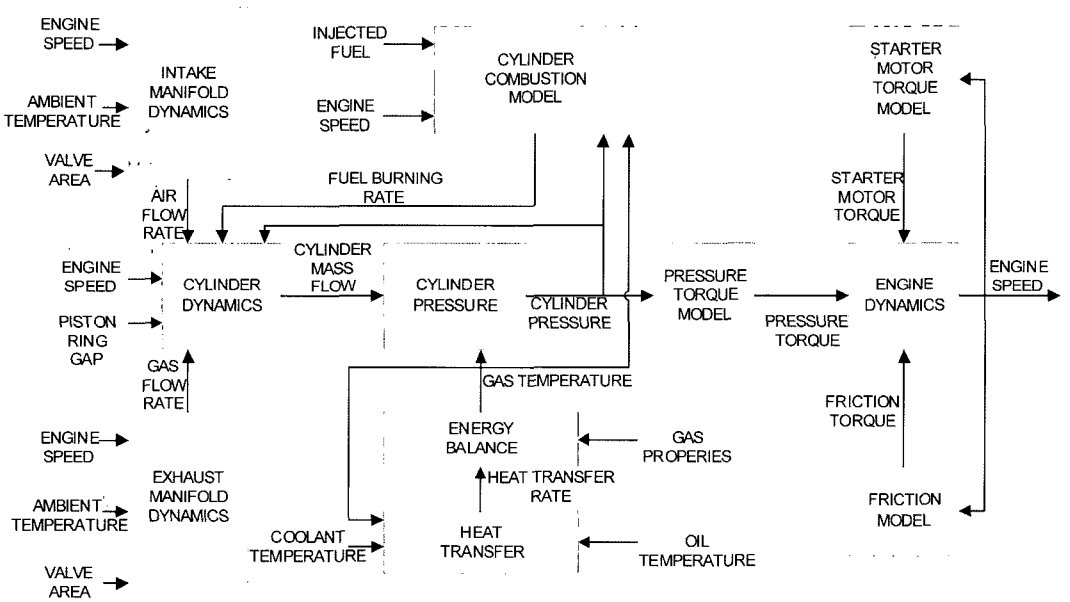

Figure 4. Block diagram of an engine and starting system for a naturally-aspirated DI diesel engine.

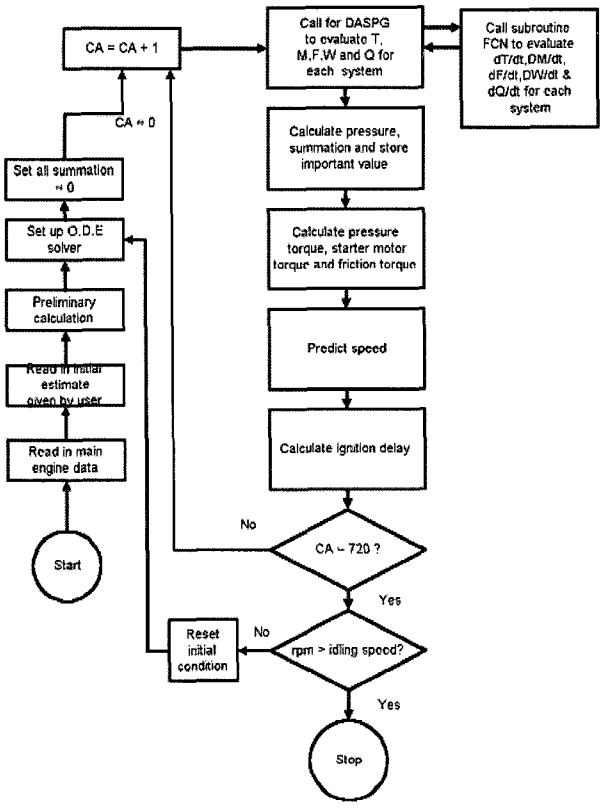

Figure 5. Program flow chart.

and mass flow rate to the cylinder make 32 equations. These 62 differential equations are solved simultaneously. The pressure of control volume can be calculated by the state equation using the given temperature and mass. To solve the overall set of differential equations, these equations are expressed in state space form, where state variables are crank angle position θ, engine speed ω, mass, temperature and equivalence ratio of intake, exhaust manifold and the individual cylinder.

In this model, using a IMSL library routine called DASPG, first order differential equations can be solved at a given initial value. This integral method can handle stiff first order differential and algebraic equation using the Petzold-Gear backward differentiation formula method. The equation is very stiff because of the difference in the electric time constant of the starter motor and the mechanical time constant of the engine.

A block diagram of an engine and a starting system model for a direct injection diesel engine is shown in Figure 4.

The necessary inputs to the simulation include engine geometry and design parameters, valve open area, starter and friction torque characteristics, initial conditions and more. The outputs are engine speed, temperature, pressure, mass and equivalence ratio of intake, exhaust manifold and cylinder, heat transfer rate and torque of the individual cylinder. The flow chart of the simulation program is shown in Figure 5.

4. RESULTS AND DISCUSSIONS

4.1. Comparison between Experimental and Simulation Results

An 8 cylinder, 736 kW, direct injection diesel engine was used to obtain the experimental data for comparison with model prediction. Basic engine specifications are given in Table 1. After all temperatures in the test engine has been stabilized at −20°C, preheating of the manifold flame torches is activated for 30 seconds. The fuel solenoid valves is opened and the fuel delivery pump directs fuel to the glow plug of a flame heater. Cranking the engine with the flame heater on but without fuel injection into the cylinder approximately lasts approximately 6 seconds. This fuel vaporized by the glow plug is mixed with engine intake air and ignited. This process warms up the intake air. Fuel is then injected into the cylinder with flame heater on. After autoignition takes place in one or more locations of the combustion chamber, full combustion starts in the premixed part of the charge which has a fuel vapor and air ratio within the rich, stoichiometric and lean ignition limits. While the starter key is on to the idle speed, approximately 1000 rpm, engine behavior was monitored. The oil temperature, coolant temperature,

Table 1. Engine specification.

Number of cylinders	8
Operating method	Four-stroke cycle
Combustion method	Diesel, Direct injection
Cylinder bore	144 mm
Stroke	140 mm
Compression ratio	14:1
Displacement, total	18.3 dm³
Injection timing	14°BTDC

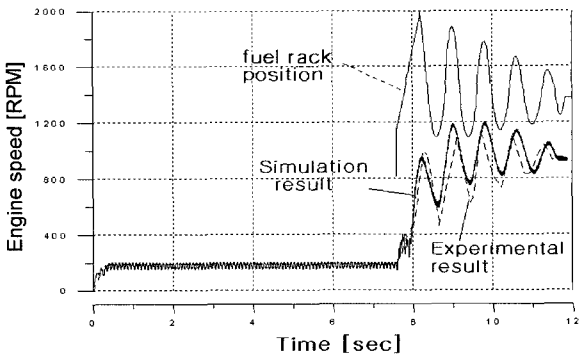

Figure 6. Engine speed variation versus time from the model and experiment.

engine speed, battery voltage and starter motor current were measured.

Figure 6 shows the simulation and the test result of engine speed from cranking, through running and warm up to idle speed with a fully-charged battery at −20°C. The dotted line represents experimental results and solid line shows simulation results. It is shown from the figure that this model describes the cranking period, transient procedure from first ignition through running and warm up period to idle speed very closely. The reason for the sudden speed drop is considered to be misfire. If misfiring is given to 5th and 7th cylinder in the calculation, the simulation results show the similar trend as compared to the experimental ones. The reason for the misfiring is not clear, but overfueling due to the high fuel rack position in this crank angle is considered to hinder combustion. During the combustion period, fuel injection rate is considered to be proportional to the fuel rack position of these test results.

Figure 7 indicates the flywheel torque given by starter motor torque versus time in cranking. The starter motor

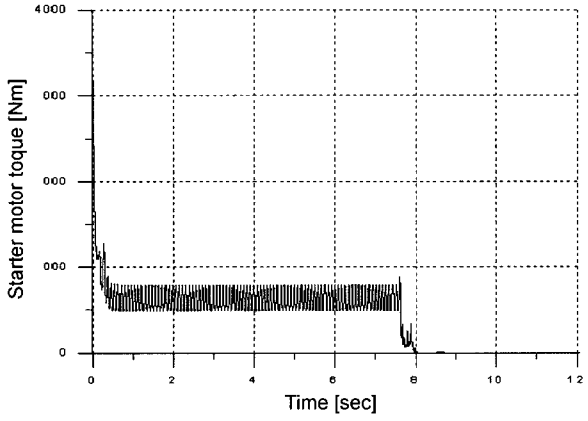

Figure 7. Starter motor torque versus time in cranking.

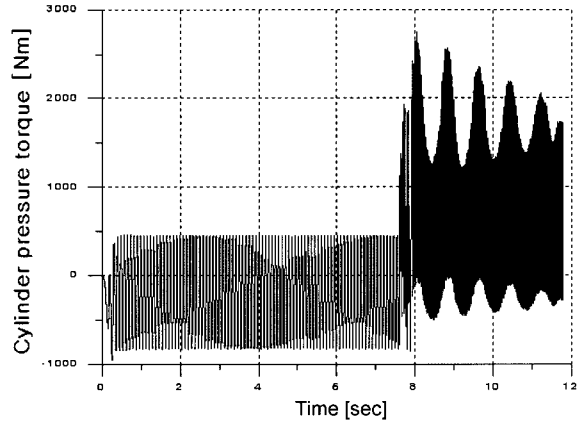

Figure 8. Cylinder pressure torque versus time in cranking.

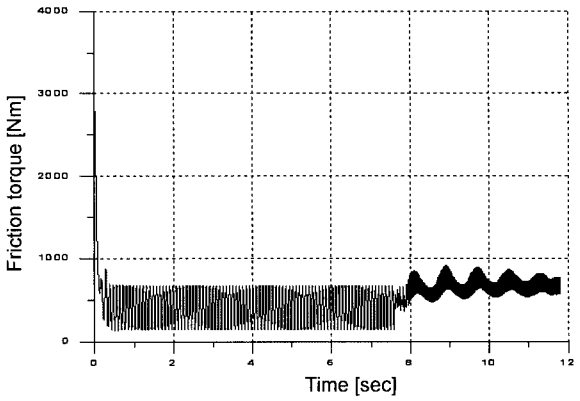

Figure 9. Engine friction torque versus time in cranking.

torque is highest at the beginning, decreases with time and eventually goes to zero when the armature current is below the threshold current. Figures 8 and 9 indicate cylinder pressure torque and friction torque variations versus time in cranking. The friction torque is considered to be the highest during the first cycle because the oil temperature is low and the oil film in the piston ring is insufficient. Friction torque during the combustion period depends heavily on engine speed and pressure. Friction torque increases as the speed and cylinder pressure increase. Inertia torque is determined by the balance of the aforementioned cylinder pressure torque, friction torque and starter motor torque. The engine cranking speed is determined within one or two cycles after cranking. In conclusion, the starter motor torque is a key factor in cold starting because cranking speed depends greatly on the starter motor torque.

4.2. Effects of Starting Variables on Cranking Process

The first autoignition greatly depends on the cylinder condition just before the fuel injection. Therefore, the cranking period without fuel injection is very important. The effects of blowby, intake air temperature increased by the flame heater, initial cylinder wall temperature and heat loss are studied by the present simulation model.

4.2.1. Effect of blowby

Figures 10 and 11 show the cylinder temperature and pressure variations versus time in crank angle during the first two cycles of the cranking process. The dotted line is for the temperature without blowby and the solid line for that with blowby. When blowby is considered, the temperature is lower and the pressure is significantly lower. During the cranking period without fuel injection, the pressure should be symmetrical by the top dead center, but because of the blowby, its shape is not symmetrical and peak pressure is reached 2~3 degrees before the top dead center.

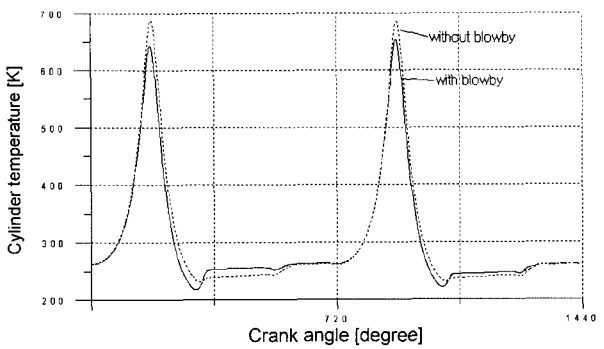

Figure 10. Cylinder temperature variation with blowby.

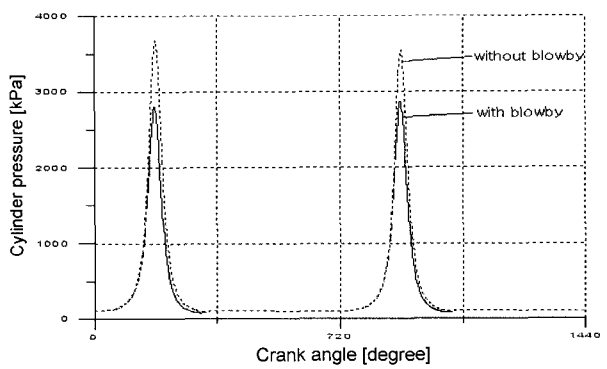

Figure 11. Cylinder pressure variation with blowby.

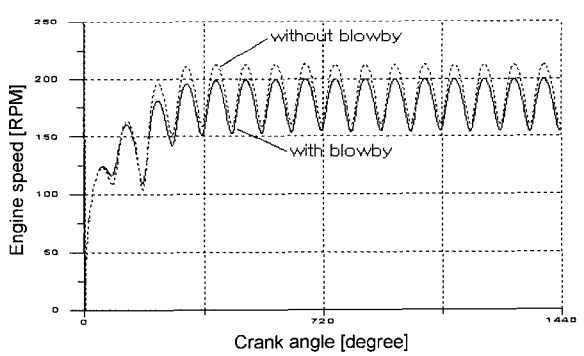

Figure 12. Engine speed variation with blowby.

Figure 12 shows that cranking speed is slower when blowby is considered. It is generally known that the blowby loss in the case of low cranking speed is larger than in the case of high speed. Therefore, there is a minimum cranking speed below which the engine would not start. That minimum varies from engine to engine and is dependent on many design variables. As mentioned before cranking speed depends greatly on the starter mortor torque.

4.2.2. Effect of air temperature

Figures 13 and 14 show cylinder tempreature and pressure variations at various intake air temperatures during

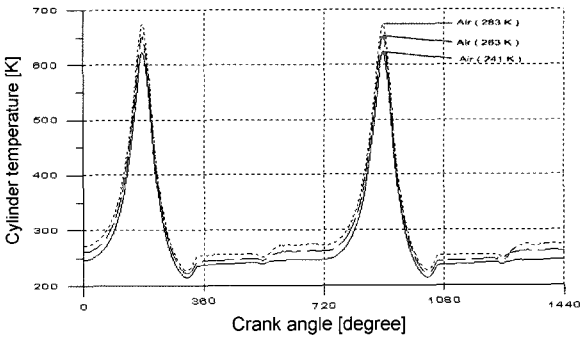

Figure 13. Cylinder temperature variation at various intake air temperature.

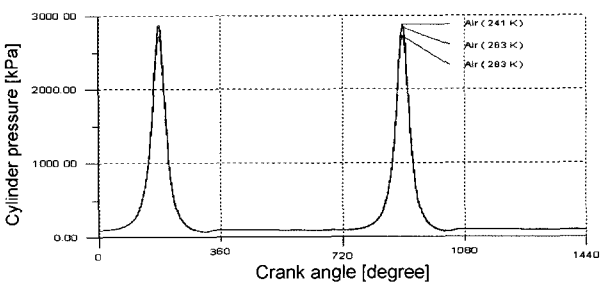

Figure 14. Cylinder pressure variation at various intake air temperature.

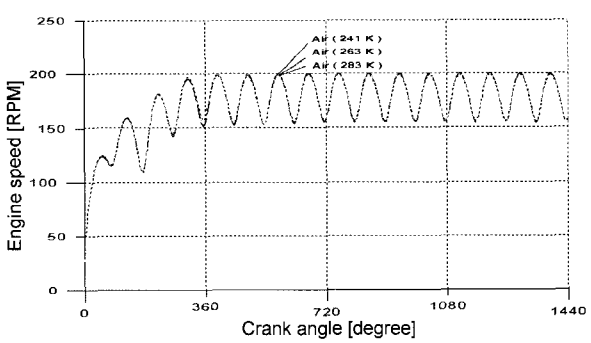

Figure 15. Engine speed variation at various intake air temperature.

the first two cycles of the cranking process. The compression temperature is significantly increased as intake air temperature increases. The compression pressure increases slowly as intake air temperature falls. This minor contribution is due to the increased initial air density which causes the pressure at intake valve closing to be higher. This overcomes reductions in the peak pressure due to the increased heat transfer. Figure 15 shows that the increase of the intake air temperature does not affect the engine cranking speed.

Therefore, the influence of intake air temperature on the compression temperature is very high. The effect of intake air temperature is probably the most important

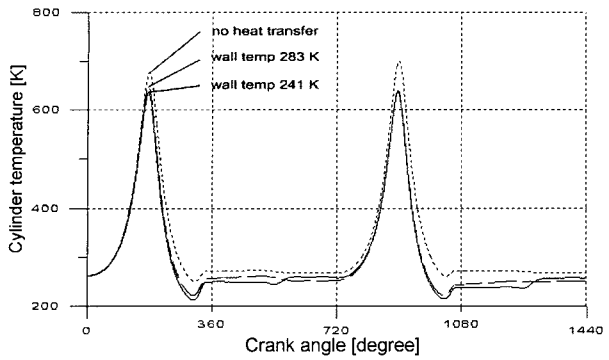

Figure 16. Cylinder temperature variation at various cylinder wall temperature.

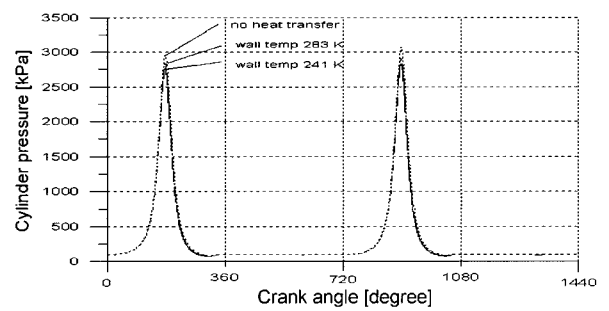

Figure 17. Cylinder pressure variation at various cylinder wall temperature.

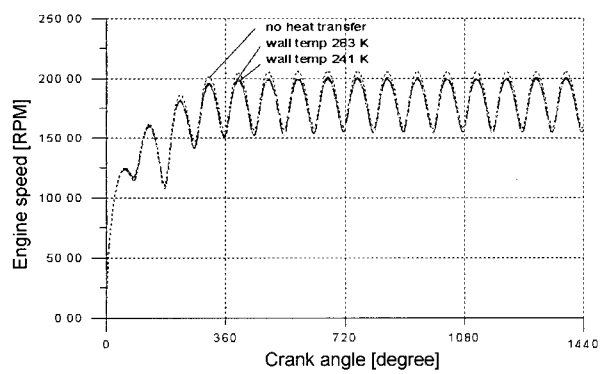

Figure 18. Engine speed variation at various cylinder wall temperature.

factor affecting the starting of a diesel engine. Intake temperature can be increased by a flame heater.

4.2.3. Effect of initial cylinder wall temperature and heat loss

Figures 16 and 17 show cylinder temperature and pressure variations at various cylinder wall temperature during the first two cycles in the cranking process. The compression temperature and pressure are increased as cylinder wall temperature increases. In particular, considerable rises in the compression temperature and pressure are possible when ignoring the heat loss.

As shown in Figure 18 cranking speed does not vary when the initial cylinder wall temperature increases from 241 K to 283 K, but a small cranking speed increase can be seen when ignoring heat loss. The initial cylinder wall temperature can be increased by the engine cooling water heater if necessary.

5. CONCLUSIONS

In this study, a dynamic model of the cold starting system of diesel engines was developed. The effects of various important factors on the cold start were studied. The results are as follows:

(1) The comparison between the calculated and experimental results generally show that the model reasonably describes the starting behavior of the test engine at −20°C.

(2) The cylinder compression temperature of the cranking process which is important in diesel engine starting is significantly influenced by starting variables such as blowby, intake air temperature, and initial wall temperature. The cylinder compression pressure and engine speed of cranking process is significantly influenced by the blowby, but not by intake air temperature and initial wall temperature.

(3) The developed model, with the inclusion of a more detailed instantaneous friction model and heat transfer model, will provide a useful tool for the optimization of the diesel engine cold starting system.

ACKNOWLEDGMENT–This paper was supported by Konkuk University in 2006.

REFERENCES

Caton, J. A. and Heywood, J. B. (1981). An experimental and analytical study of heat transfer in an engine exhaust port. *Int. J. Heat Mass Transfer* **24**, **4**, 581–595.

Gardner, T. P. and Henein, N. A. (1988). Diesel starting: A mathematical model. *SAE Paper No.* 880426.

Heywood, J. B. (1988). *Internal Combustion Engine Fundamentals*. McGraw-Hill. New York. 750–784.

Hiroyasu, H., Kadota, T. and Arai, M. (1980). Supplementary comments: Fuel spray characterization in diesel engines. *Combustion Modeling in Reciprocating Engines,* Plenum Press, 369–408.

Liu, H., Henein, N. A. and Nryzik, W. (2003). Simulation of diesel engines cold-start. *SAE Trans.* **112**, **3**, 352–372.

Liu, H. Q., Chalhoub, N. G. and Henein, N. (2001). Simulation of a single cylinder diesel engine under cold start conditions using simulink. *J. Engineering for*

Gas Turbine and Power, **123**, 117–123.
Medica, V. and Giadrossi, A. (1994). Numerical simulation of turbocharged diesel engine operation in transient load conditions. *ASME Trans. Eng. Syst. Des. Anal.* PD-Vol. 64-8. 3, ASME, New York, 589–596.
Namazian, M. and Heywood, J. B. (1982). Flow in the piston-cylinder-ring crevices of a spark ignition engine: Effect on hydrocarbon emissions, efficiency and power. *SAE Paper No.* 820088.
Olikara, C. and Borman, G. L. (1975). A computer program for calculating properties of equilibrium combustion products with some applications to I.C. engines. *SAE Paper No.* 75046.
Poublon, M. and Patterson, D. J. (1985). Instantaneous crank speed variations as related to engine starting. *SAE Paper No.* 850482.
Rezeka, S. F. and Henein, N. A. (1984). A new approach to evaluate instantaneous friction and its components in internal combustion engines. *SAE Paper No.* 840179.
Rogenberg, R. C. (1982). General friction considerations for engine design. *SAE Paper No.* 821576.
Shin, K. B., Brennan, M. J., Joe, Y-G. and Oh, J-E. (2004). Simple models to investigate effect of velocity dependent friction on the disc brake squeal noise. *Int. J. Automotive Technology* **5**, **1**, 1–67.
Tang, D.-L., Sutan, M. C. and Chang, M.-F. (1989). A dynamic engine starting model for computer-aided control systems design. *ASME Book No.* H00546, 203–222.
Uras, H. M. and Patterson, D. J. (1985). Oil and ring effects on piston-ring assembly friction by the instantaneous IMEP method. *SAE Paper No.* 850440.
Watson, N., Pilley, A. D. and Marzouk, M. (1980). A combustion correlation for diesel engines simulation. *SAE Paper No.* 800029.
Woschni, G. (1967). Universally applicable equation for the instantaneous heat transfer coefficient in the internal combustion engine. *SAE Paper No.* 670931.

APPENDIX A

This appendix provides the expressions for the friction torque of various engine components, $T_f^{(i)}$ terms defined by Rezeka and Henein (1984). The friction torque induced by the hydrodynamic lubrication regime of the piston rings is given by

$$T_f^{(1)} = [\mu S_p w(P_{gas} + P_e)]^{0.5} D(n_o + 0.4n_c) r T_k \quad \text{(A1)}$$

where μ is oil film viscosity, S_p is average piston speed, w is ring width, P_e is elastic pressure of the ring, D is cylinder bore, n_o is number of oil rings, n_c is number of compressions rings, r is crank radius, and T_k is a dummy number indicating the angle of the crank. The friction torque due to the mixed lubrication regime at the piston rings is

$$T_f^{(2)} = \pi D n_c w(P_{gas} + P_e)(1 - |\sin\theta|) r T_k \quad \text{(A2)}$$

The friction torque resulting from the hydrodynamic lubrication regime of the piston skirt is

$$T_f^{(3)} = \mu v_p D L_{ps} r T_k / h_o \quad \text{(A3)}$$

where h_o is clearance between the piston skirt and cylinder liner, and L_{ps} is length of piston skirt. The valve train friction torque is

$$T_f^{(4)} = G L_s r T_k / \sqrt{\omega} \quad \text{(A4)}$$

where G is number of intake and exhaust valves per cylinder, L_s is the spring load, and ω is the instantaneous angular velocity of the crankshaft. The auxiliaries and unloaded bearing friction torque are defined as

$$T_f^{(5)} = \mu\omega \quad \text{(A5)}$$

The loaded bearing friction is obtained from

$$T_f^{(6)} = \frac{\pi}{4} D^2 r_c P_{gas} |\cos\theta| / \sqrt{\omega} \quad \text{(A6)}$$

where r_c is journal bearing radius.

APPENDIX B

This appendix provides the expressions for the heat transfer coefficients between the gas and the wall in cylinder and ports. This cylinder heat transfer coefficient (kW/m^2 K) is defined as

$$\alpha = 130 D^{m-1} P^m T^{0.75-1.62m} W^m \quad \text{(B1)}$$

The exponent m is selected to be 0.8, which corresponds to turbulent fluid flow in pipes. The average cylinder gas velocity W determined for a four-stroke, water-cooled, four-valve direct-injection CI engine without swirl are expressed as follows:

$$W = \left[C_1 S_p + C_2 \frac{V_d T_r}{P_r V_r} (P - P_o) \right]$$

where S_p is the mean piston speed, V_d is displaced volume, P is the instantaneous cylinder pressure, P_r, V_r, T_r are the working-fluid pressure, volume and temperature at the reference state, and P_o is the motored cylinder pressure at the same crank angle. The first term in the bracket reflects the effect of the piston on the average gas velocity in the cylinder and the second term in the bracket accounts for the additional gas velocity induced by the combustion. For the gas exchange period:

C_1=6.18, C_2=0

For the compression period:

C_1=2.28, C_2=0

For the combustion and expansion period:

C_1=2.28, C_2=3.24×10^{-3} m/sec°C

The port heat transfer coefficient is calculated by using the Caton and Heywood's correlation (1981). For valve open period

$$Nu=0.35\mathrm{Re}_j^{0.6} \quad \text{(B2)}$$

where $\mathrm{Re}_j=v_jD_v/v$, D_v is the valve diameter, v_j is the velocity of jet through the valve opening, and v is the kinematic viscosity. For valve closed period

$$Nu = 0.022\mathrm{Re}_D^{0.8} \quad \text{(B3)}$$

here $\mathrm{Re}_D=v_pD_p/v$, where v_p is the time-averaged port gas velocity and D_p is the port diameter.